Relationship between the Atmospheric CO₂ and Climate Indices by Wavelet-Based Multifractal Analysis

Fumio Maruyama

Department of Sport and Health Science, Matsumoto University, Matsumoto, Japan
Email: fmaruya@nagoya-u.jp

Abstract

Atmospheric concentrations of greenhouse gases are rising, leading to a positive radiative forcing of climate and an expected warming of surface temperatures. In general, fractal properties may be observed in the time series of the dynamics of complex systems. To study the relation between the atmospheric CO_2 concentration and the climate indices, we investigated the change of fractal behavior of the CO_2, the carbon isotope ratio ($\delta^{13}C$) of atmospheric CO_2, the El Niño-Southern Oscillation (ENSO), the Pacific Decadal Oscillation (PDO), and the North Atlantic Oscillation (NAO) indices using the multifractal analysis. When the atmospheric CO_2 growth rate was large, the multifractality of CO_2, $\delta^{13}C$ in CO_2, ENSO, and NAO was large and the changes were large from the change of fractality. The changes of CO_2 and ENSO were closely related and the influence of the CO_2 on the ENSO was strong from the change in fractality and wavelet coherence. When the El Niño occurred, the CO_2 growth rate was large. The CO_2 related to PDO, NAO, and global temperature from the change in fractality and wavelet coherence. Especially, the changes of CO_2 and global temperature were closely related. When the global warming hiatus occurred, the multifractality of the global temperature was weaker than that of CO_2 and the change of the global temperature was stable. These findings will contribute to the research of the relation between the atmospheric CO_2 and climate change.

Keywords

Atmospheric CO_2, $\delta^{13}C$, ENSO, PDO, NAO, Wavelet, Multifractal

1. Introduction

Atmospheric concentrations of greenhouse gases are rising, leading to a positive

radiative forcing of climate and an expected warming of surface temperatures.

Many of the El Niño events appear to be associated with a net transfer of CO_2 from the biosphere to the atmosphere. ENSO events produce droughts, particularly in tropical regions, which can cause drought and forest fires and increase CO_2 (Keeling et al., 1995; Langenfelds et al., 2002).

The North Atlantic Oscillation (NAO) and the Pacific-North America (PNA) indices are correlated with the observed atmospheric CO_2 growth rate (Murayama et al., 2004).

Various objects in nature show the so-called self-similarity or fractal property. Monofractal shows a roughly similar pattern at different scales and is characterized through a fractal dimension. Multifractal is a non-uniform, more complex fractal and is separated into many sub-sets characterized through different fractal dimensions. Fractal property can be observed in the time series representing dynamics of complex systems as well. A change of fractality occurs with a phase transition and changes of state. The multifractal properties of daily rain were studied in two contrasting climates: an East Asian monsoon climate with drastic rain variability and a mild climate with moderate rain variability (Svensson et al., 1996). In both the climates, the frontal rain shows monofractality and the convective-type rain shows multifractality.

Hence, climate change can be interpreted from the view of fractals. A change of fractality may be observed when the climate changes. We use the wavelet transform to analyze the multifractal behavior of the climate index. Wavelet methods are useful for the analysis of complex non-stationary time series. The wavelet transform allows good multifractal analysis to be performed (Muzy et al., 1991). We used the wavelet transform to analyze the multifractal behavior of the climate index. We concluded that a climatic regime shift corresponds to a change from multifractality to monofractality of the Pacific Decadal Oscillation (PDO) index (Maruyama et al., 2015).

To study the relation between the atmospheric CO_2 concentration and the climate indices, we investigated the change of multifractal behavior of the CO_2, the carbon isotope ratio ($\delta^{13}C$) of atmospheric CO_2, the Southern Oscillation Index (SOI), and the NAO index using the multifractal analysis.

2. Data and Method of Analysis

The SOI, Niño3.4, PDO, NAO indices, and global mean surface air temperature anomalies provided by NOAA's Climate Prediction Center, USA (CPC) were used. The SOI is a standardized index based on the observed sea level pressure differences between Tahiti and Darwin, Australia. The SOI is one measure of the large-scale fluctuations in air pressure occurring between the western and eastern tropical Pacific (i.e., the state of the Southern Oscillation) during El Niño and La Niña episodes. Prolonged periods of negative (positive) SOI values coincide with abnormally warm (cold) ocean waters across the eastern tropical Pacific typical of El Niño (La Niña) episodes.

Atmospheric CO_2 concentrations (ppm) derived from in situ air measurements at Mauna Loa, Observatory, Hawaii was used. Monthly atmospheric ^{13}C concentrations (per mil) in CO_2 derived from flask air samples at Mauna Loa Observatory was used. Annual mean growth rate of CO_2 for Mauna Loa obtained from NOAA was used.

For the examination, we used the Daubechies wavelet, which is widely used in solving a broad range of problems, e.g., self-similarity properties of a signal and signal discontinuities. We made use of a discrete signal that was fitted the Daubechies mother wavelet with the capacity of correct inverse transformation. Thus, we can precisely calculate the following best $\tau(q)$, which can be regarded as a characteristic function of the fractal behavior. We can define the $\tau(q)$ from the power-law behavior of the partition function, as shown in equation (2). We then computed the scaling of the partition function $Z_q(a)$, which is defined as the sum of the q-th powers of the modulus of the wavelet transform coefficients at scale a, where q is the q-th moment. In our computation, the wavelet-transform coefficients did not grow zero. Thus, for a correct calculation, the summation was considered for the whole set. Muzy et al. (1991) defined $Z_q(a)$ as the sum of the q-th powers of the local maxima of the modulus to avoid dividing by zero. We got the following partition function $Z_q(a)$:

$$Z_q(a) = \sum \left| W_\varphi[f](a,b) \right|^q \tag{1}$$

where $W_\varphi[f](a,b)$, a and b are the wavelet coefficient of function f, a scale parameter, and a space parameter, respectively. $W_\varphi[f](a,b)$ is defined as below.

$$W_\varphi[f](a,b) = \frac{1}{\sqrt{|a|}} \int_{-\infty}^{+\infty} f(t)\phi^*\left(\frac{t-b}{a}\right)dt \tag{2}$$

where $f(t)$ is data and φ is wavelet function. For small scales, we expect

$$Z_q(a) \sim a^{\tau(q)} \tag{3}$$

First, we examined the changes in $Z_q(a)$ in the time series at a different scale a for each moment q. We plotted the logarithm of $Z_q(a)$ against that of time scale a. Here $\tau(q)$ is the slope of the fitted straight line for each q. Next, we plotted $\tau(q)$ versus q. The time window was advanced by one year, which was repeated. The time window was fixed to 6 years, when a moderate change in fractality was observed. Monofractal and multifractal signals were defined as follows. For $\tau(q)$, a monofractal signal corresponds to a straight line, while a multifractal signal is nonlinear (Frish & Parisi, 1985). We calculated the R^2 value, which is the coefficient of determination, for the fitted straight line. If $R^2 \geq 0.98$, the time series is monofractal and if $0.98 > R^2$, it is multifractal.

We calculated the $\tau(q)$ of different moments q for individual records in the Niño3.4 index. In Figure 1, the $\tau(q)$ between 1980 and 1994 is shown. The data were analyzed in six-year sets, e.g., $\tau(q)$ of n80 was calculated between 1980 and 1985, and that of n81 was calculated between 1981 and 1986. To investigate the change of fractality, the time window was then shifted forward one year and $\tau(q)$
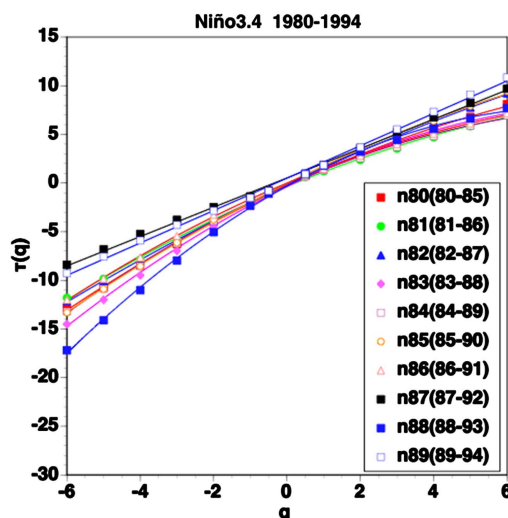
Figure 1. $\tau(q)$ for individual Niño3.4 index between 1980 and 1994.

was calculated from n80 up to n89. A monofractal signal would correspond to a straight line for $\tau(q)$, while a multifractal signal would be nonlinear. Nearly all the multifractality observed is due to the negative value of q, i.e., small fluctuations are more inhomogeneous than large fluctuations. In Figure 1, the data sets were monofractal in the cases of n80, n81, n82, n85, n86, n87, and n89 and were multifractal in the cases of n83, n84, and n88.

We plotted the value of the $\tau(-6)$ in each index. The negative large values of the $\tau(-6)$ show large multifractality. For the $\tau(q)$, $q = -6$ is the appropriate number to show the change of τ.

3. Results

3.1. The Relation between the Atmospheric CO_2 and $\delta^{13}C$ in CO_2

The time series of atmospheric CO_2 and $\delta^{13}C$ in CO_2 are shown in Figure 2. Changes in $\delta^{13}C$ of CO_2 can be used in global carbon-cycle models to elucidate the relative reles of oceanic and terrestriall uptake of fossil-fuel CO_2 (Francey et al., 1985). The CO_2 increased and $\delta^{13}C$ decreased with time, hence there was an inverse relationship between CO_2 and $\delta^{13}C$, which indicated that these changes were mainly generated by activities of terrestrial biosphere.

We investigated the relation between the CO_2 and $\delta^{13}C$. The $\tau(-6)$ of the CO_2, and $\delta^{13}C$ are shown in Figure 3 (top). The red square shows monofractality and the green circle shows multifractality for the 6 years centered on the year plotted. For instance, the green circle for 1980 in the CO_2 shows multifractality between 1977 and 1982. The data was excluded from Figure 3 (top) for cases where we could not distinguish between monofractality and multifractality. The changes in fractality of the CO_2 and $\delta^{13}C$ were inverse for 1995-2010, which corresponded to the change of the CO_2 and $\delta^{13}C$ in CO_2. When the CO_2 growth rate was large as shown in 3.2, the $\tau(-6)$ of $\delta^{13}C$ was small and the multifractality was large. The changes of CO_2 and $\delta^{13}C$ in CO_2 were related to each other.

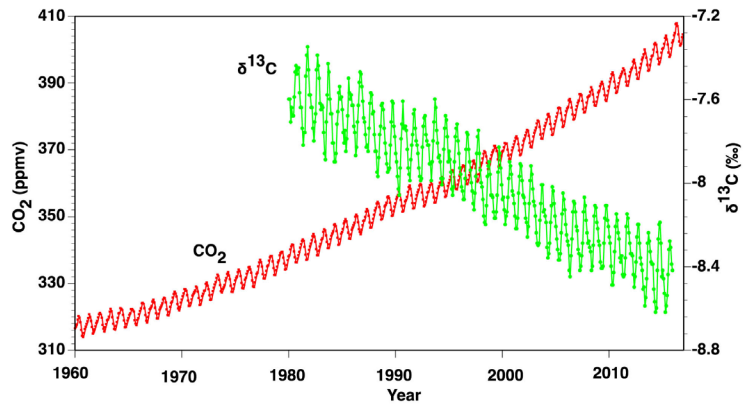**Figure 2.** The time series of CO_2 and $\delta^{13}C$ in CO_2.
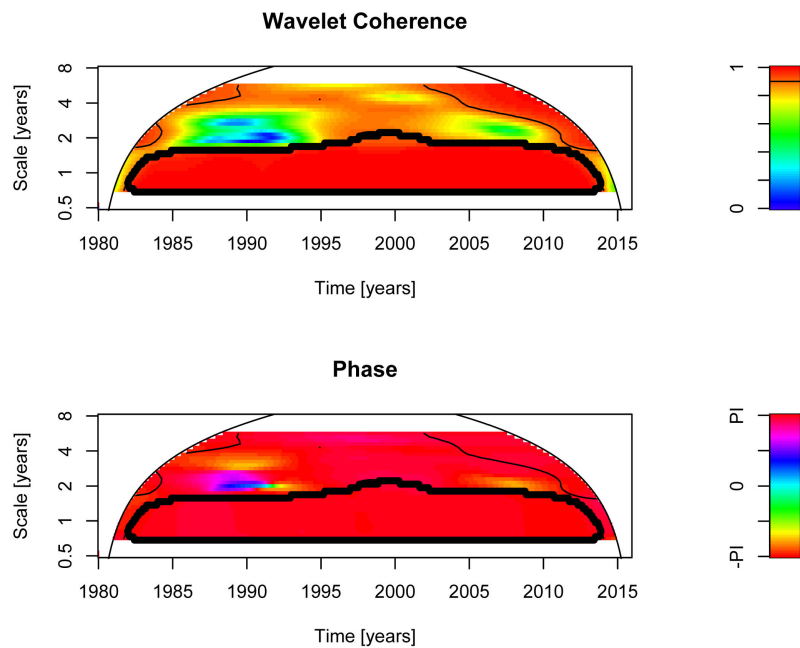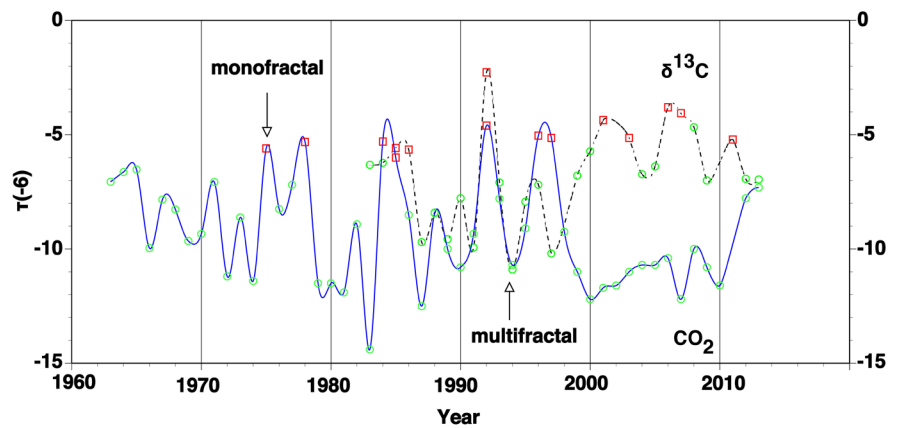

Figure 3. The $\tau(-6)$ of CO_2 and $\delta^{13}C$ in CO_2 (top). Wavelet coherence (middle) and phase (bottom) between the CO_2 and $\delta^{13}C$ in CO_2. In the wavelet phase, the positive value shown by the blue and pink shading means that the CO_2 leads the $\delta^{13}C$ and the negative value shown by the green, yellow and red shading means that the $\delta^{13}C$ leads the CO_2.

We studied the relationship between the CO_2 and $\delta^{13}C$ by means of wavelet coherence. We show the wavelet coherence and phase using the Morlet wavelet between the CO_2 and $\delta^{13}C$ in Figure 3 (middle) and (bottom), respectively. The coherence between the CO_2 and $\delta^{13}C$ in 1 - 2 year scale was very strong for 1980-2010, when the changes of the fractality both were very similar and the phase of CO_2 was delayed by π from the $\delta^{13}C$.

3.2. The Relation between the CO_2 Growth Rate and the Multifractality of CO_2

We investigated the relation between the annual mean CO_2 growth rate and the multifractality of CO_2. The annual mean CO_2 growth rate for Mauna Loa and the $\tau(-6)$ of the CO_2 are shown in Figure 4. The changes of the CO_2 growth rate and the $\tau(-6)$ of CO_2 were very similar. When the CO_2 growth rate was large, the $\tau(-6)$ of the CO_2 was small and multifractality was large. When the El Niño (65 - 66, 72 - 73, 82 - 83, 86 - 87, 94 - 95, 97 - 98, 02 - 03, 09 - 10) occurred, the CO_2 growth rate was large. When the La Niña (73 - 74, 75 - 76, 99 - 00, 07 - 08) occurred, the CO_2 growth rate was small.

3.3. The Relation between the CO_2 and ENSO

We investigated the relation between the CO_2 and SOI. The $\tau(-6)$ of the CO_2, and SOI are shown in Figure 5 (top). The changes in fractality of the CO_2 and SOI were very similar for 1965-2010 especially for the 1970s and 1990s. When the CO_2 growth rate was large, the ENSO event occurred and the $\tau(-6)$ of SOI was small and multifractal was strong. The changes of CO_2 and ENSO were related to each other. We studied the relationship between the CO_2 and SOI by means of wavelet coherence. We show the wavelet coherence and phase using the Morlet wavelet between the CO_2 and SOI in Figure 5 (middle) and (bottom), respectively. The coherence between the CO_2 and SOI in two year scale was strong for 1970-2000, when the changes in the fractality both were very similar and the lead of the CO_2 was observed. The proportion of eastern versus central Pacific-type El Niño events increases with CO_2 (Stevenson et al., 2012).
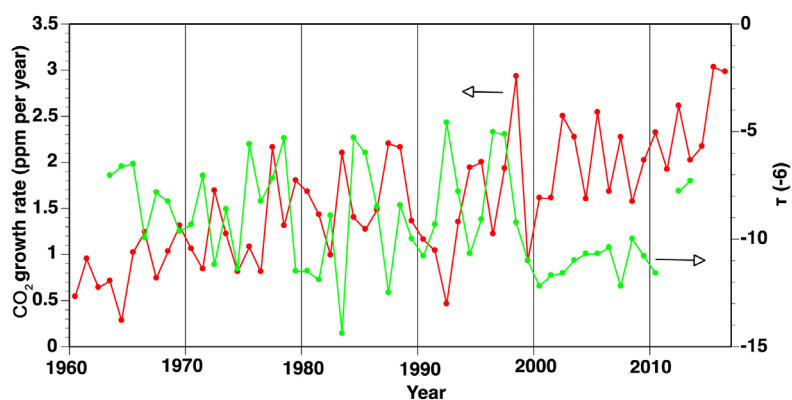

Figure 4. The annual mean CO_2 growth rate for Mauna Loa (red) and the $\tau(-6)$ of the CO_2 (green).
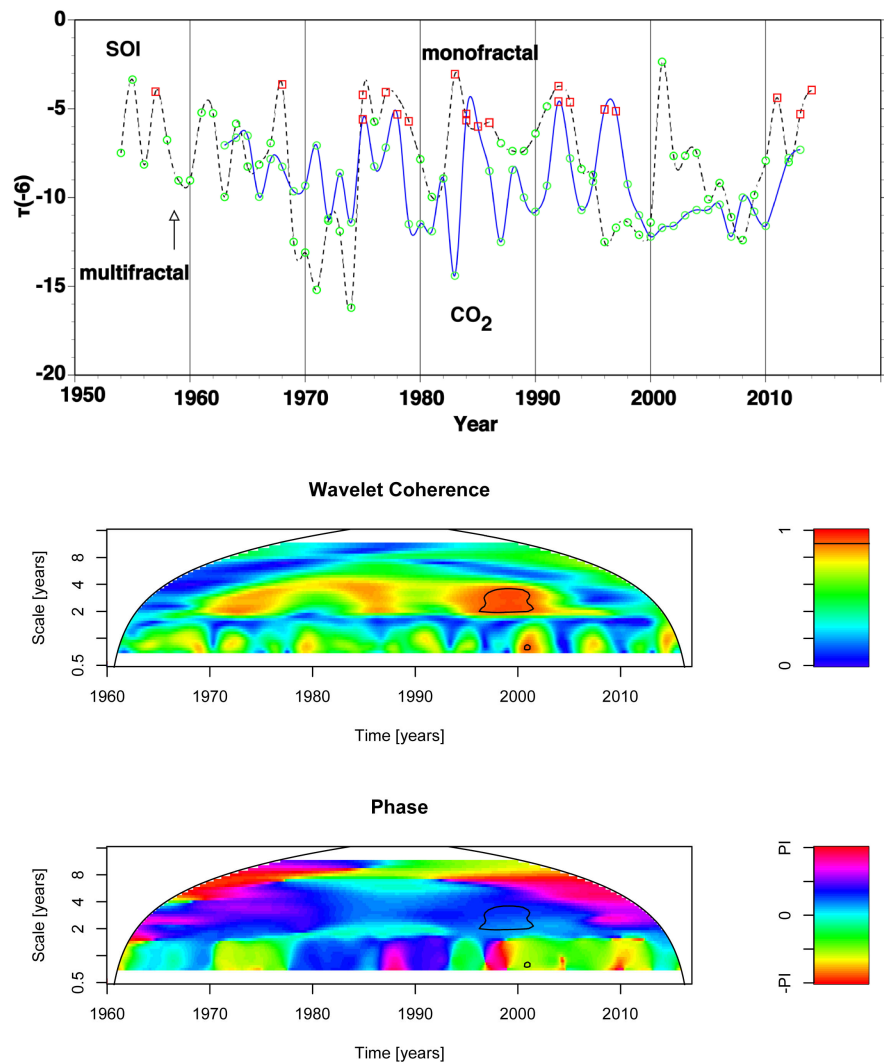
43

Figure 5. The $\tau(-6)$ of CO_2, and SOI (top). Wavelet coherence (middle) and phase (bottom) between the CO_2 and SOI. In the wavelet phase, the positive value shown by the blue and pink shading means that the CO_2 leads the SOI and the negative value shown by the green, yellow and red shading means that the SOI leads the CO_2.

We investigated the relation between the CO_2 and Niño3.4. The $\tau(-6)$ of the CO_2, and Niño3.4 are shown in **Figure 6** (top). The changes in fractality of the CO_2 and Niño3.4 were very similar for 1970-1995. When the CO_2 growth rate was large, the ENSO event occurred and the $\tau(-6)$ of Niño3.4 was small and multifractal was strong. The changes of CO_2 and ENSO were related to each other. We show the wavelet coherence and phase using the Morlet wavelet between the CO_2 and Niño3.4 in **Figure 6** (middle) and (bottom), respectively. The coherence between the CO_2 and Niño3.4 in one year scale was strong for 1960-2010, when the lead of the CO_2 was observed.

3.4. The Relation between the CO_2 and PDO

We investigated the relation between the CO_2 and PDO. The $\tau(-6)$ of the CO_2,
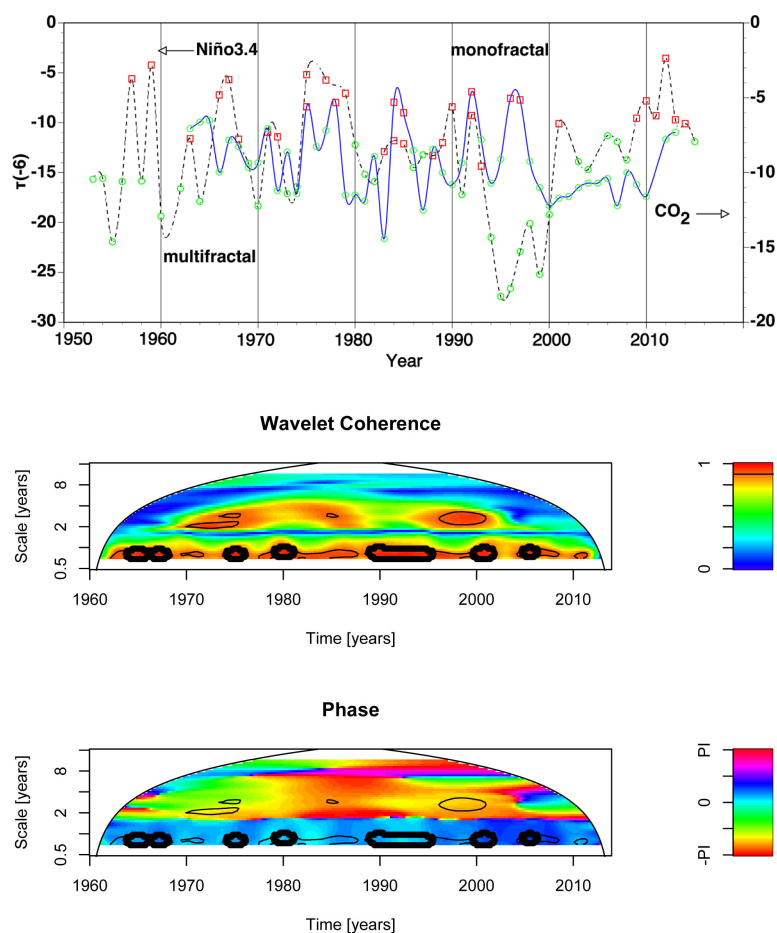
Figure 6. The $\tau(-6)$ of CO_2 and Niño3.4 (top). Wavelet coherence (middle) and phase (bottom) between the CO_2 and Niño3.4. In the wavelet phase, the positive value shown by the blue and pink shading means that the CO_2 leads the Niño3.4 and the negative value shown by the green, yellow and red shading means that the Niño3.4 leads the CO_2.

and PDO are shown in **Figure 7** (top). The changes in fractality of the CO_2 and PDO were very similar for 1965-2010, especially for the 1970s and 1990s. The changes of CO_2 and PDO were related to each other.

We studied the relationship between the CO_2 and PDO by means of wavelet coherence. We show the wavelet coherence and phase using the Morlet wavelet between the CO_2 and PDO in **Figure 7** (middle) and (bottom), respectively. The coherence between the CO_2 and PDO in 1 - 2 year scale was strong for the 1990s, when both the changes in fractality were very similar and the lead of the PDO was observed.

3.5. The Relation between the CO_2 and NAO

We investigated the relation between the CO_2 and NAO. The $\tau(-6)$ of the CO_2, and NAO are shown in **Figure 8** (top). The changes in fractality of the CO_2 and NAO were very similar for 1960-2000. When the CO_2 growth rate was large, the $\tau(-6)$ of NAO was small and multifractal was strong. The changes of CO_2 and NAO were related to each other.
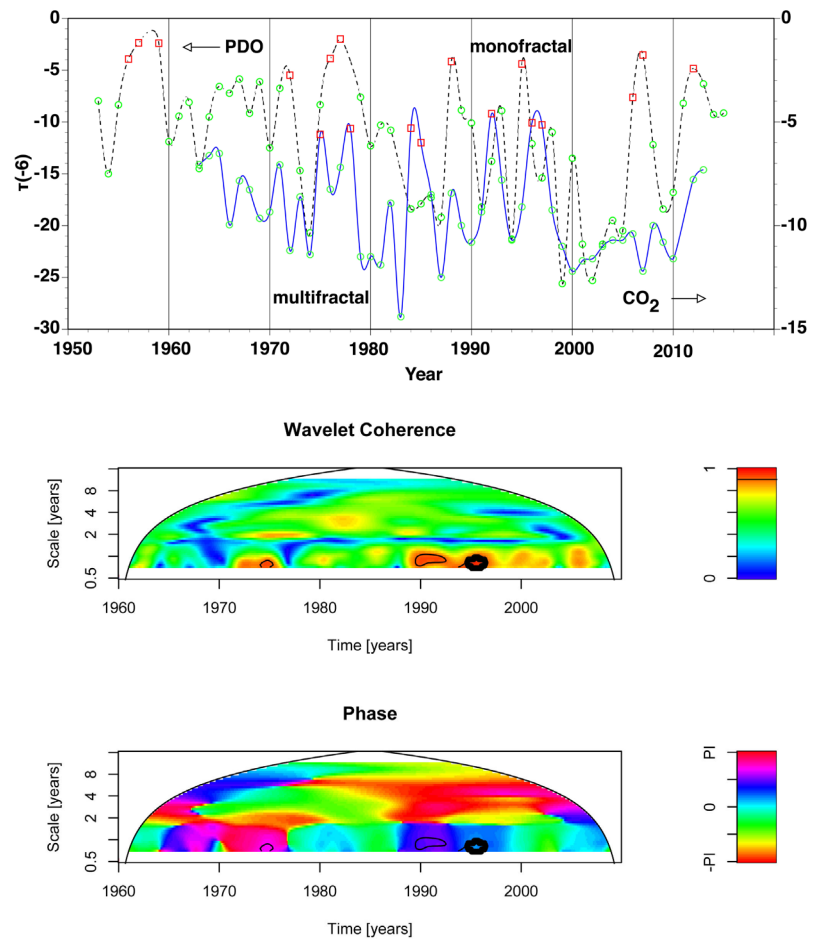
Figure 7. The $\tau(-6)$ of CO_2 and PDO (top). Wavelet coherence (middle) and phase (bottom) between the CO_2 and PDO. In the wavelet phase, the positive value shown by the blue and pink shading means that the CO_2 leads the PDO and the negative value shown by the green, yellow and red shading means that the PDO leads the CO_2.

We studied the relationship between the CO_2 and NAO by means of wavelet coherence. We show the wavelet coherence and phase using the Morlet wavelet between the CO_2 and NAO in **Figure 8** (middle) and (bottom), respectively. The coherence between the CO_2 and NAO in one year scale was strong, and the lead of the CO_2 and NAO was observed.

3.6. The Relation between the Atmospheric CO_2 and Global Temperature

We investigated the relation between the CO_2 and global temperature. The global mean surface temperature anomalies is shown in **Figure 9**. The rate of global temperature increase slowed during 1950-1975 and 1998-2012. The change between 1998 and 2012 was often termed the "global warming hiatus" (Medhang et al., 2017). The $\tau(-6)$ of the CO_2, and global temperature are shown in **Figure 10** (top). The changes in fractality of the CO_2 and global temperature were very similar for 1970-2000, when the rate of global temperature increased largely. The changes of CO_2 and global temperature were related to each other.
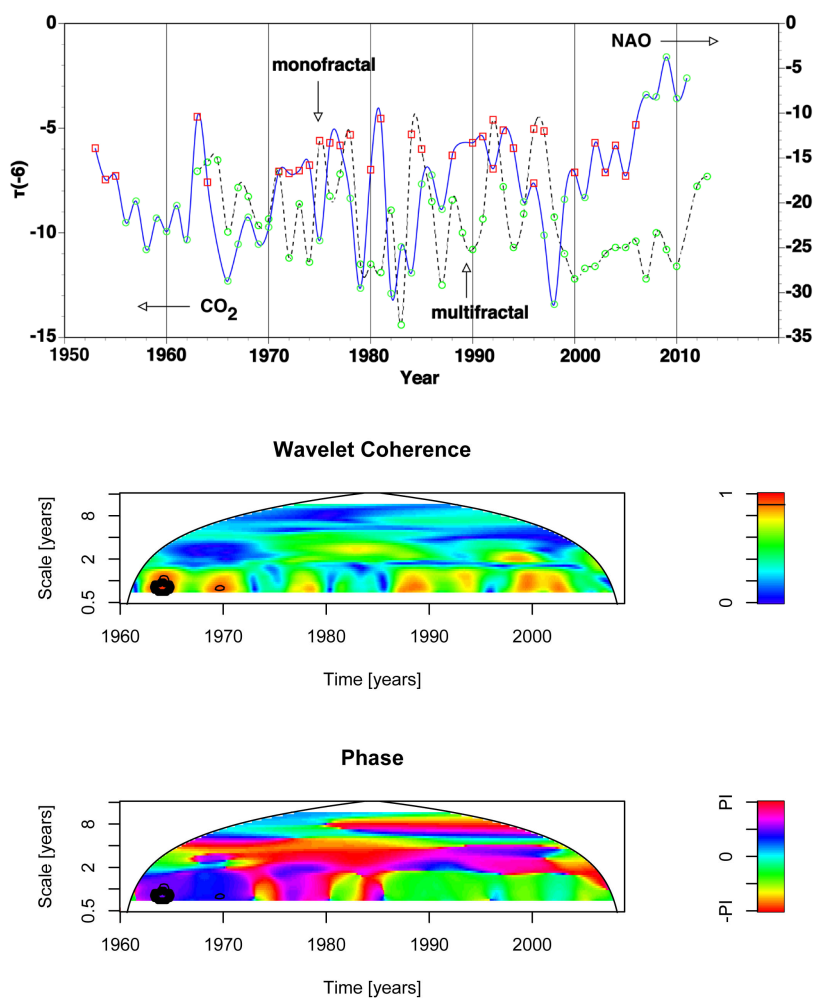
Wavelet Coherence

Phase

Figure 8. The $\tau(-6)$ of CO_2, and NAO (top). Wavelet coherence (middle) and phase (bottom) between the CO_2 and NAO. In the wavelet phase, the positive value shown by the blue and pink shading means that the CO_2 leads the NAO and the negative value shown by the green, yellow and red shading means that the NAO leads the CO_2.
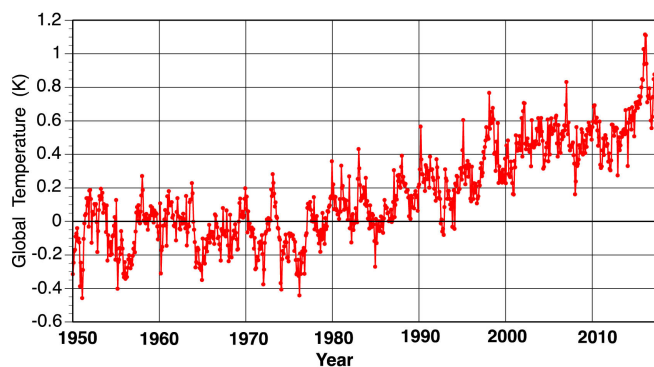

Figure 9. Global mean surface temperature anomalies.

We studied the relationship between the CO_2 and global temperature by means of wavelet coherence. We show the wavelet coherence and phase using the Morlet wavelet between the CO_2 and global temperature in **Figure 10**
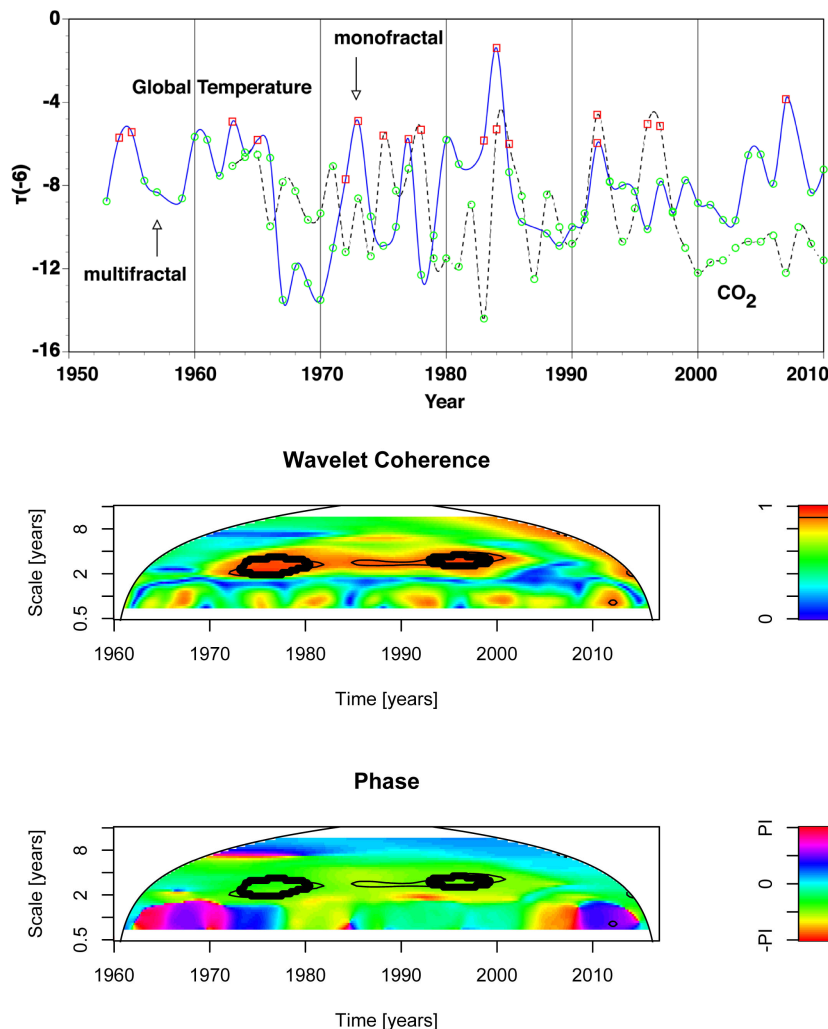
Figure 10. The $\tau(-6)$ of CO_2, and global temperature (top). Wavelet coherence (middle) and phase (bottom) between the CO_2 and global temperature. In the wavelet phase, the positive value shown by the blue and pink shading means that the CO_2 leads the global temperature and the negative value shown by the green, yellow and red shading means that the global temperature leads the CO_2.

(middle) and (bottom), respectively. The coherence between the CO_2 and global temperature in two year scale was very strong, when the rate of global temperature increased largely. The lead of the global temperature was observed.

4. Discussion

4.1. The Influence of the $\delta^{13}C$ on the CO_2 Concentration

The CO_2 increased and $\delta^{13}C$ decreased with time, so there was an inverse relationship between CO_2 and $\delta^{13}C$, which indicated that these changes were mainly generated by activities of terrestrial biosphere. The $\delta^{13}C$ decreased due to combustion of fossil fuel with isotopically light CO_2 (Nakazawa et al., 1993).

When the CO_2 growth rate was large, the $\tau(-6)$ of the CO_2 was small and multifractality was large and the change was large. The changes in fractality of the

CO_2 and $\delta^{13}C$ were very similar for 1985-2010. When the CO_2 growth rate was large, the $\tau(-6)$ of $\delta^{13}C$ was small and the multifractality was large. The changes of CO_2 and $\delta^{13}C$ in CO_2 were closely related.

4.2. The Influence of the ENSO, PDO, NAO, and Global Temperature on the CO_2 Concentration

The changes in fractality of the CO_2 and SOI were very similar for 1965-2010. The coherence between the CO_2 and SOI in 2 - 4 year scale was strong for 1970-2000 and the lead of the CO_2 was observed. The CO_2 differences between the central and western Pacific Ocean correlate well with the SOI. There is more (less) midtropospheric CO_2 in the central Pacific and less (more) midtropospheric CO_2 in the western Pacific during El Niño (La Nina) events (Jiang et al., 2013). When the CO_2 growth rate was large, the ENSO event occurred and the $\tau(-6)$ of SOI was small and multifractal was strong. The changes of CO_2 and ENSO were closely related. The influence of the CO_2 on the ENSO (SOI and Niño3.4) was strong from the change of fractality and wavelet coherence. When the El Niño (La Niña) occurred, the CO_2 growth rate was large (small). The relationship between the CO_2 and the SOI values is shown (Matsueda et al., 2015).

The changes in fractality of the CO_2 and PDO were very similar for 1965-2010 especially for the 1970s and 1990s and the changes of CO_2 and PDO were related to each other. The changes in fractality of the CO_2 and NAO were very similar for 1965-2000. The coherence between the CO_2 and NAO in one year scale was strong and the leads of the CO_2 and NAO were observed. When the CO_2 growth rate was large, the $\tau(-6)$ of NAO was small and multifractality was strong. The changes of CO_2 and NAO were related to each other. When the rate of global temperature increased largely, the changes in fractality of the CO_2 and global temperature were very similar and the coherence between the CO_2 and global temperature was very strong. For 1998-2012 (global warming hiatus), the multifractality of the global temperature was weaker than that of CO_2. The change of the global temperature was more stable than that of CO_2. The changes of CO_2 and global temperature were closely related. Hence, the CO_2 related to PDO, NAO, and global temperature from the change in fractality and wavelet coherence.

5. Conclusion

To study the relation between the atmospheric CO_2 concentration and the climate indices, we investigated the change of fractal behavior of the CO_2, the carbon isotope ratio ($\delta^{13}C$) of atmospheric CO_2, SOI, Niño3.4, PDO, and NAO indices using the multifractal analysis. We showed the change of factuality by plotting the τ-function and used the wavelet coherence. The main findings are summarized below.

1) When the atmospheric CO_2 growth rate was large, the multifractality of CO_2, $\delta^{13}C$ in CO_2, ENSO, and NAO was large and the changes were large from the change of fractality.

2) The changes of CO_2 and ENSO were closely related and the influence of the CO_2 on the ENSO was strong from the change in fractality and wavelet coherence. When the El Niño occurred, the CO_2 growth rate was large.

3) The CO_2 related to PDO, NAO, and global temperature from the change in fractality and wavelet coherence. Especially, the changes of CO_2 and global temperature were closely related. When the global warming hiatus occurred, the multifractality of the global temperature was weaker than that of CO_2 and the change of the global temperature was stable.

These findings will contribute to the research of the relation between the atmospheric CO_2 and climate change.

Conflicts of Interest

The author declares no conflicts of interest regarding the publication of this paper.

References

Francey, R. J., Tans, P. P., Allison, C. E., Enting, I. G., White, J. W. C., & Trolier, M. (1985). Changes in Oceanic and Terrestrial Carbon Uptake Since 1982. *Nature, 373,* 326-330. https://doi.org/10.1038/373326a0

Frish, U., & Parisi, G. (1985). On the Singularity Structure of Fully Developed Turbulence. In M. Ghil, R. Benzi, & G. Parisi (Eds.), *Turbulence and Predictability in Geophysical Fluid Dynamics and Climate Dynamics* (pp. 84-88). New York: North-Holland.

Jiang, X., Wang, J., Olsen, E. T., Liang, M., Pagano, T., Chen, L. L., Licata, S. J., & Yung, Y. L. (2013). Influence of El Niño on Midtropospheric CO_2 from Atmospheric Infrared Sounder and Model. *Journal of the Atmospheric Sciences, 70,* 223-230.

Keeling, C. D., Whorf, T. P., Wahlen, M., & Plichtt, J. V. D. (1995). Interannual Extremes in the Rate of Rise of Atmospheric Carbon Dioxide Since 1980. *Nature, 375,* 666-670. https://doi.org/10.1038/375666a0

Langenfelds, R. L., Francey, R. J., Pak, B. C., Steele, L. P., Lloyd, J., Trudinger, C. M., & Allison, C. E. (2002). Interannual Growth Rate Variations of Atmospheric CO_2 and Its $D^{13}C$, H_2, CH_4, and CO between 1992 and 1999 Linked to Biomass Burning. *Global Biogeochemical Cycles, 16,* 21-1-21-22. https://doi.org/10.1029/2001GB001466

Maruyama, F., Kai, K., & Morimoto, H. (2015). Wavelet-Based Multifractal Analysis on Climatic Regime Shifts. *Journal of the Meteorological Society of Japan, 93,* 331-341.

Matsueda, H., Machida, T., Sawa, Y., & Niwa, Y. (2015). Long-Term Changes of CO_2 Latitudinal Distribution in the Upper Troposphere. *Geophysical Research Letters, 42,* 2508-2514.

Medhang, I., Stolpe, M. B., Fischer, E. M., & Knutti, R. (2017). Reconciling Controversies about the "Global Warming Hiatus". *Nature, 545,* 41-47. https://doi.org/10.1038/nature22315

Murayama, S., Taguchu, S., & Higuchi, K. (2004). Interannual Variation in the Atmospheric CO_2 Growth Rate: Role of Atmospheric Transport in the Northern Hemisphere. *Journal of Geophysical Research Atmospheres, 109,* D02305.

Muzy, J. F., Bacry, E., & Arneodo, A. (1991). Wavelets and Multifractal Formalism for Singular Signals: Application to Turbulence Data. *Physical Review Letters, 67,* 3515-3518. https://doi.org/10.1103/PhysRevLett.67.3515

Nakazawa, T., Morimoto, S., Aoki, S., & Tanaka, M. (1993). Time and Space Variations of the Carbon Isotopic Ratio of Tropospheric Carbon Dioxide over Japan. *Tellus, 45B,*

258-274. https://doi.org/10.3402/tellusb.v45i3.15728

Stevenson, S., Fox-Kemper, B., & Jochum, M. (2012). Understanding the ENSO-CO_2 Link Using Stabilizes Climate Simulations. *Journal of Climate, 25,* 7917-7936. https://doi.org/10.1175/JCLI-D-11-00546.1

Svensson, C., Olsson, J., & Berndtsson, R. (1996). Multifractal Properties of Daily Rainfall in Two Different Climates. *Water Resources Research, 32,* 2463-2472. https://doi.org/10.1029/96WR01099